In-concert immune dynamics during natural influenza virus infection and recovery in acute hospitalized patients

Thi H.O. Nguyen[1], Marios Koutsakos[1], Carolien E. van de Sandt[1,2], Jeremy Chase Crawford[3], Liyen Loh[1], Sneha Sant[1], Ludivine Grzelak[4], Emma K. Allen[3], Tim Brahm[3], E. Bridie Clemens[1], Maria Auladell[1], Luca Hensen[1], Zhongfang Wang[1], Simone Nüssing[1], Xiaoxiao Jia[1], Patrick Günther[1], Adam K. Wheatley[1], Stephen J. Kent[1,5,6], Malet Aban[7], Yi-Mo Deng[7], Karen L. Laurie[7], Aeron C. Hurt[7], Stephanie Gras[8,9], Jamie Rossjohn[8-10], Jane Crowe[11], Jianqing Xu[12], David Jackson[1], Lorena E. Brown[1], Nicole La Gruta[8], Weisan Chen[13], Peter C. Doherty[1], Stephen J. Turner[14], Tom C. Kotsimbos[15,16], Paul G. Thomas[3], Allen C. Cheng[17,18*#] and Katherine Kedzierska[1*#]

Affiliations

[1]Department of Microbiology and Immunology, University of Melbourne, at the Peter Doherty Institute for Infection and Immunity, Parkville 3010, Victoria, Australia.

[2]Department of Hematopoiesis, Sanquin Research and Landsteiner Laboratory, Amsterdam UMC, University of Amsterdam, 1066CX, Amsterdam, Netherlands.

[3]Department of Immunology, St Jude Children's Research Hospital, Memphis 38105, Tennessee, USA.

[4]Biology Department, École Normale Supérieure Paris-Saclay, Université Paris-Saclay Cachan 94230, France.

[5]Melbourne Sexual Health Centre and Department of Infectious Diseases, Alfred Hospital and Central Clinical School, Monash University, Melbourne 3004, Victoria, Australia.

[6]ARC Centre for Excellence in Convergent Bio-Nano Science and Technology, University of Melbourne, Parkville 3010, Victoria, Australia.

[7]World Health Organisation (WHO) Collaborating Centre for Reference and Research on Influenza, at The Peter Doherty Institute for Infection and Immunity, Melbourne 3000, Victoria, Australia.

[8]Department of Biochemistry and Molecular Biology, Biomedicine Discovery Institute, Monash University, Clayton 3800, Victoria, Australia.

[9]Australian Research Council Centre of Excellence for Advanced Molecular Imaging, Monash University, Clayton 3800, Victoria, Australia.

[10]Institute of Infection and Immunity, Cardiff University School of Medicine, Heath Park, Cardiff CF14 4XN, United Kingdom.

[11]Deepdene Surgery, Deepdene 3103, Victoria, Australia.

[12]Shanghai Public Health Clinical Centre and Institutes of Biomedical Sciences, Key Laboratory of Medical Molecular Virology of Ministry of Education/Health, Shanghai Medical College, Fudan University, Shanghai 201508, China.

[13]Department of Biochemistry and Genetics, La Trobe Institute of Molecular Science, La Trobe University, Bundoora 3084, Victoria, Australia.

[14]Department of Microbiology, Biomedicine Discovery Institute, Monash University, Clayton 3800, Victoria, Australia.

[15]Department of Allergy, Immunology and Respiratory Medicine, The Alfred Hospital, Melbourne 3004, Victoria, Australia.

[16]Department of Medicine, Monash University, Central Clinical School, The Alfred Hospital Melbourne 3004, Victoria, Australia.

[17]School of Public Health and Preventive Medicine, Monash University, Melbourne 3004, Victoria, Australia.

[18]Infection Prevention and Healthcare Epidemiology Unit, Alfred Health, Melbourne 3004, Victoria, Australia.

KLL is currently at Seqirus, Parkville 3052, Victoria, Australia.

[*]These authors contributed equally.

[#]Corresponding authors: kkedz@unimelb.edu.au; allen.cheng@monash.edu.

Abstract

We report in-concert dynamics of 18 key immune parameters, related to clinical, genetic and virological factors, in patients hospitalized with influenza across different severity levels. Influenza disease was associated with correlated increases in IL6/IL-8/MIP-1α/β cytokines and lower antibody responses. Robust activation of circulating T follicular helper cells (cTfhs) correlated with peak antibody-secreting cells (ASC) and influenza heamaglutinin-specific memory B-cell numbers, which phenotypically differed from vaccination-induced B-cell responses. Influenza-specific $CD8^+$/$CD4^+$ T-cells increased early in disease and remained activated during patient recovery. Here, we describe the broadest to-date immune cellular networks underlying recovery from influenza infection, highly relevant to other infectious diseases.

Millions of people are hospitalized with severe influenza disease annually. In 2017, an estimated 9.5 million people globally were hospitalized with influenza virus lower respiratory tract infections, for a total of 81.5 million days[1]. Moreover, an estimated 243,000-645,000 of seasonal influenza-associated respiratory deaths occur annually[2]. Although seasonal influenza virus infections can cause debilitating illness leading to hospitalization and death[3], viral, host and immune factors determining the disease severity are unclear, as are the precise mechanisms of why some individuals present with a mild 'asymptomatic' infection, while others, including previously healthy or vaccinated individuals, succumb to severe viral pneumonia and fatal influenza disease. Increased susceptibility to influenza virus infection and exacerbation of disease severity can reflect an overactivation of the innate immune system, leading to hypercytokinemia, alveolar oedema and pulmonary complications, and/or impaired humoral and cellular immunity, delaying the recovery phase. While neutralizing antibodies can reduce disease transmission and viral load, the current vaccination regimens targeting antibody responses[4] are often short-lived and directed against specific influenza strains, thus not protective against unpredicted influenza viruses.

Based on human studies of natural and experimental influenza virus infection, it is well-established that in the absence of neutralizing antibodies, pre-existing memory $CD8^+$ T cells and $CD4^+$ T cells can reduce disease severity[5-14]. Published evidence also associates genetic host factors, such as specific HLA types and interferon-induced transmembrane protein 3 (IFITM3) single-nucleotide polymorphisms (SNPs) with clinically poor outcomes[15-18]. The IFITM3 rs12252-C/C genotype along with early detection of inflammatory mediators IL-6, IL-8, IL-10 and MIP-1β measured in the blood within 48 hours of hospital admission, were associated with fatal disease outcomes in our 2013 study of hospitalized H7N9-infected patients in China (n=18 patients, 12 recovered, 6 died)[18]. In contrast, recovery from severe H7N9 infection was associated with lower cytokine levels and prominent $CD8^+$ T cell responses[18]. Inflammatory serum cytokines IL-6 and IL-8 have also been linked to severe seasonal and pandemic influenza virus infections in hospitalized adult patients[19] and predicted hospitalization in a household cohort of naturally-infected individuals, including infants, children and adults[20]. In critically-ill children, higher levels of blood cytokines (IL-6, IL-8, IP-10, GM-CSF, MCP-1, and MIP-1α) measured within 72 hours of ICU admission correlated with fatal influenza virus infection[21].

There is scant data on the main drivers of severe influenza resulting in hospitalization or death[22,23]. Previous studies of influenza-infected patient cohorts mainly focused on a very select number of immunological parameters, with only three studies combining innate (cytokines/monocytes/NK cells) and adaptive T cell immunity[12,24,25], and two other studies incorporating innate immunity, T cell immunity and antibody responses[10,26]. The limited number of parameters measured is often due to a difficulty in obtaining longitudinal samples from acutely-infected patients combined with the amount of biological material required per assay. Only one other study, the SHIVERS report[26] analysed convalescent samples 2 weeks post-enrolment (along with one acute sample) and showed prolonged immune activation of innate and adaptive cellular responses in hospitalized patients compared to non-hospitalized patients.

Thus, there is a clear deficiency in our understanding of the specific interplay between genetics, innate and adaptive immune responses driving recovery from acute viral pneumonia.

Here, we utilized longitudinal samples obtained from patients hospitalized with acute influenza disease to elucidate how innate and adaptive immune responses work in concert to resolve influenza disease. We report, at a very high level of resolution, the overall breadth and kinetics of 18 key immune parameters: the antiviral/inflammatory cytokines and chemokines, hemagglutinin (HA)-directed antibodies, HA-probe-specific B cells, antibody-secreting cells (ASCs), circulatory $CD4^+$ T follicular helper (cTfh) cells, influenza peptide/MHC-specific $CD8^+$ and $CD4^+$ T cells, IFN-γ-producing $CD8^+$ T cells, $CD4^+$ T cells, Natural Killer (NK) cells, Mucosal-associated invariant T (MAIT) and γδ T cells, and granzymes A, B, K, M and perforin expression in $CD8^+$, $CD4^+$, NK and MAIT cells. This comprehensive panel of immune parameters, combined with host genetic factors and patient clinical data, enabled a detailed dissection of human factors driving susceptibility, severity and recovery in patients hospitalized with seasonal influenza viruses, highly relevant to other infectious diseases, especially newly-emerging respiratory infections.

Results

Patient DISI cohort

We recruited 64 patients admitted to the Alfred Hospital (Prahran, Australia) between 2014-2017 into our "Dissection of Influenza-Specific Immunity" (DISI) cohort. The inclusion criteria for the DISI study included hospital admission of consenting adult patients with influenza-like illness (ILI). The longitudinal study involved serial blood and nasal swab samples collected from influenza-PCR-positive patients (Flu+, *n*=44) within 1-2 days of hospital admission to discharge and follow-up blood samples ~30 days later, allowing analyses of the recovery phase (**Fig. 1a**). Patients who were influenza-PCR-negative (Flu-, *n*=20) were included as ILI-matched controls. The DISI cohort included one patient #11 who became infected with H3N2 while in hospital with AML, and died 34 days later from febrile neutropenia. We also had one death in the control group, patient #28 who was PCR-negative at admission, but subsequently became IBV-PCR-positive while in hospital and died 61 days later in ICU. The remaining cohort was admitted to the Respiratory/General Ward with one case patient #62 requiring 1 day in ICU. 53 patients presented with ILI, while 6 cases and 1 control patient presented with pneumonia (**Supplementary Tables 1 and 2)**.

We successfully recalled 80% (35/44) of Flu+ patients at a median of 41 days after disease onset and 75% of our Flu- patients (15/20, median 39 days). Overall, Flu+ patients were predominantly (55%) infected with the H3N2 influenza A virus (IAV) subtype (**Fig. 1b** and **Supplementary Table 1**), followed by the co-circulating IAV 2009 pandemic H1N1 (pH1N1)-like strain (16%) and two co-circulating influenza B virus (IBV) strains (Phuket/3073/2013 (9%) and Brisbane/60/2008 (7%)), representing the dominant strains for each year in Australia. IAV-infected patients (median 58 yrs, *n*=34) were significantly older than IBV-infected (45 yrs, *n*=10) and Flu- patients (47 yrs, *n*=20) (**Fig. 1c**). Apart from age, patient demographics in Flu+ and Flu- groups were well-matched, with 86% and 70%, respectively, having one or more high-risk conditions for severe influenza disease. Both groups had a median of 4 days in hospital (**Supplementary Tables 1-2**). Time in hospital was significantly lower than that for more severely-ill H7N9 cohort[18] with a median 14 days for recovery (n=12, p<0.0001) and a median of 33 days for those who died (n=6, p=0.0239) (**Fig. 1d**). The lower hospital burden reflects the lower severity of seasonal influenza compared to avian A/H7N9 disease.

Risk HLA class-I and IFITM3-SNPs do not contribute to disease severity in hospital settings

To determine whether the risk HLA class-I and IFITM3-SNPs genetic factors contributed to influenza disease severity in hospitalized patients, we compared HLA type and IFITM3 SNP alleles between Flu+ and Flu- patients. HLA types (**Supplementary Table 2**) were grouped according to "universal" or "risk" alleles based on studies describing HLA-A*02:01/03:01 and HLA-B*08:01/18:01/27:05/57:01 molecules binding universally conserved influenza peptides[27],

versus HLA-A*24:02/68:01 types positively correlating with pH1N1 mortality[15] and morbidity[16]. Given that our cohort was mainly Caucasian (82% Flu+, 95% Flu-, **Supplementary Table 1**), the frequencies of universal and risk alleles were comparable between two groups (**Fig. 1e**). Similarly, for IFITM3 SNP analyses, the non-risk rs12252-T/T homozygous allele was observed in 91% of Flu+ patients (remaining were C/T heterozygous) and 100% of Flu- patients, whereas the risk C/C homozygous allele was absent (**Fig. 1f**). The rs34481144 SNP showed a higher frequency of the A/G-heterozygous allele for both groups (41% and 50%, respectively), with equal or similar proportions of the risk A/A and non-risk G/G homozygous alleles (**Fig. 1g**). Further analyses of Flu+ patients with the risk A/A rs34481144 SNP versus Flu+ patients with A/G-heterozygous allele and non-risk G/G homozygous alleles showed no differences in disease severity in hospital settings, as measured by sequential (sepsis-related) organ failure assessment (SOFA) scores[28] (**Fig. 1h**).

Highly correlated cytokines cluster together during influenza virus infection

Hypercytokinemia of early inflammatory mediators (IL-6, IL-8, IL-10, MCP-1, MIP-1α and MIP-1β) have been associated with an increase in disease severity causing death in a number of hospitalized cohorts[18-21]. Pro-inflammatory cytokines and chemokines measured in the blood of acute representative Flu+ patients showed increased cytokine levels, particularly IL-6 and IL-8, between mild and moderate patients as defined by lower (0-1) or higher (2-6) SOFA scores, respectively, and in the more severe patient requiring ICU support (**Fig. 1i).** Heightened IL-6 levels were also associated with the more severe 2013 H7N9-infected patients (**Fig. 1i**)[18]. After adjusting for age and the sampling time after days of disease onset, IL-6, IL-8, MIP-1α and MIP-1β were significantly, strongly positively correlated with each other early after infection at V1 timepoint. This inter-correlated cytokine cluster was still strongly present at convalescence, with less significant correlations with other cytokines/chemokines (**Fig. 1j**). Therefore, our data support previous reports that IL-6, IL-8, MIP1α and MIP-1β serve as biomarkers for severe influeza disease.

Antibody responses increase in magnitude and breadth at convalescence

The annual influenza vaccine is provided for free for high-risk groups under the National Immunisation Program. Despite the high proportion of Flu+ patients in this cohort being defined as high-risk due to pre-exisiting comorbidities (86%), only 48% of these patients were vaccinated against influenza prior to infection, compared to 65% of Flu- patients (**Supplementary Table 1**). There was rapid antigenic drifting of the H3N2 viruses between 2014-2017, with more annual updates of the H3-HA vaccine component compared to the less variable H1-HA and B-HA components (**Supplementary Table 3**). Rapid drift of the H3N2 component was evident in the viral HA-sequence analyses of nasal swabs from H3N2-infected patients with sufficient RNA. All 12 H3N2 viruses isolated from patients, including 9 who had been vaccinated, were from a different H3N2 clade when compared to the current H3N2 seasonal vaccine strain (**Fig. 2a**). Conversely, fewer H1-HA and B-HA sequence variations were observed between isolates from the infected patients compared to the WHO reference strains (**Supplementary Fig. 1**). Interestingly, despite the H3N2 clade-mismatches, all H3N2-infected patients (except one A/unsubtyped patient) generated HA inhibition (HAI) antibody titres of 40 and above (equivalent to $\log_2(HAI/10)\geq 2$) against the H3 vaccine strain (same year as infection) at follow-up, compared to 54% at acute timepoints (**Fig. 2b**), suggesting a boost in strain-specific antibodies that may have contributed to the significant increase in vaccine-strain titres ($p<0.0001$). However, only marginal increases in antibody titres were observed in H1- and B-infected patients at follow-up (**Fig. 2b**). Geometric mean titres (GMT) were low for all three H1, H3 and B subtypes during acute infection, but their ability to mount antibody responses at follow-up was generally comparable to vaccine-induced responses in a healthy cohort but with greater GMT fold-changes (**Fig. 2c,d**). As expected, antibody titres were low and remained unchanged in the Flu- group (**Fig. 2c,d**).

Previous exposures to past influenza strains, influenced by age, can affect our immune responses to current influenza virus infections[29]. To study the breadth of antibody responses,

HAI antibody landscapes were generated against current and older influenza strains from the last century that the patients may have previously encountered (**Supplementary Table 3**). Antibody responses to past strains were minimal during acute infection (V1 and V2) (**Fig. 2e,f**). However, at follow-up, Flu+ patients induced robust antibody responses to older strains from the same subtype that they were infected with, a phenomenon known as back-boosting[29], but not against the other subtypes (**Fig. 2e,f**). Therefore, compared to the Flu- and healthy cohorts, Flu+ patients started with lower antibody titres at hospitalization, perhaps due to lower vaccine coverage, but were able to mount robust and broad antibody responses at convalescence.

Activation of cTfh, ASCs and influenza-specific memory B cells prior to recovery

Tfh cells are essential for generating high-affinity memory B cells in germinal centers (GCs) and are located in secondary lymphoid organs[30]. cTfh cells share phenotypic and functional properties to GC Tfh cells, and we and others showed that inactivated influenza vaccination (IIV) induces expansion and PD-1/ICOS-activation of $CD4^+CXCR5^+CXCR3^+$ cTfh type-1 (cTfh1) cells, which correlated with antibody and $CD19^+CD27^{++}CD38^{++}$ ASC responses[4,31].

Here, we show for the first time that activated $PD\text{-}1^+ICOS^+$ cTfh1 cells emerged within influenza-infected patients in parallel with ASC responses, both peaking between days 7-10 after disease onset in both Flu+ and Flu- groups, prior to patients' recovery. cTfh1 cells peaked higher in Flu+ patients compared to Flu- groups, as shown by the separation of the 95% confidence intervals (**Fig. 3a-c, Supplementary Fig. 2a**). The number of ASCs was significantly higher (~2-8 fold) during acute infection compared to follow-up for both Flu+ and Flu- groups (**Fig. 3d**). Overall, activated cTfh1 cells were also trending higher at acute compared to follow-up (~2 fold, p=0.0519, Mann-Whitney test, **Fig. 3e**). Specifically, numbers of activated cTfh1 cells in Flu+ patients were significantly higher than the cTfh2 and cTfh17 subsets, at both acute and follow-up timepoints (**Fig. 3e**). Further, cTfh1 responses strongly correlated with ASC responses during acute influenza virus infection (**Fig. 3f**), but less so for cTfh2 and cTfh17 subsets (**Supplementary Fig. 3**). Acute ASC responses also correlated with high antibody responses ($\log_2$(HAI/10)$\geq$2 or HAI$\geq$40, **Fig. 3g**). However, acute cTfh responses did not significantly correlate with antibody responses, perhaps due to the low titres observed in some patients during acute infection, in contrast to a vaccination response where IIV-induced cTfh1 responses correlated with the fold-change in antibody titres (d28 over d0 baseline)[4].

To evaluate influenza-specific memory B cell responses during natural influenza virus infection in comparison to vaccination, recombinant HA probes relevant to the 2014-2017 vaccine strains were used to detect class-switched IgD^- HA-specific B cells in Flu+ patients (**Fig. 3h, Supplementary Fig. 2b**). These rHA probes have been extensively validated for their specificity[4,32,33]. Numbers of rHA^+IgD^- B cells in total and per probe did not significantly change between acute and follow-up timepoints (**Fig. 3i**), and were comparable to the magnitudes observed following IIV[4]. Phenotype and isotype distributions of the total B cells remained stable between acute and follow-up timepoints (**Fig. 3j,k**). Specifically, rHA^+IgD^- B cells for H3 and B probes were more $CD21^{lo}CD27^{hi}$ activated memory in proportion at the acute timepoint compared to follow-up (H3: p=0.0007, B: p=0.0017), before becoming more $CD21^{hi}CD27^{hi}$ resting memory at follow-up compared to acute timepoints (H3: p=0.0004, B: p<0.0001) (**Fig. 3j,l** top panels). Conversely, in a healthy vaccinated cohort, the resting memory phenotype was most prominent at baseline, before becoming more activated memory from days 7-28 following IIV (**Fig. 3m**, top panel). The isotype distribution in Flu+ patients was enriched for IgG^-IgM^- cells (mostly IgA^+) for H3, and IgA^+ cells for the B-probe at acute timepoints, before becoming largely IgG^+ at follow-up for each probe (**Fig. 3j,l** bottom panels). In contrast, the isotype distribution of rHA^+IgD^- B cells did not change in healthy donors following IIV (**Fig. 3m**, bottom panel). Thus, our analyses show striking differences after influenza virus infection compared to vaccination of recruited rHA^+IgD^- B cells at both phenotypic and isotype levels.

Although patients' HA-specific B cell responses did not positively correlate with their acute antibody responses which were generally low, there was a significant positive correlation between activated or resting memory HA-specific B cells with their acute ASC response, as well as resting memory HA-specific B cells with the acute cTfh responses (**Supplementary Fig. 4**).

Taken together, we show prominent activation of cTfh1 cells during acute influenza virus infection, at the time of the ASC and influenza-specific memory B cell responses.

Influenza-specific adaptive CD8$^+$ and CD4$^+$ T cells respond early after infection

Our previous work showed that rapid recovery from severe A/H7N9 was associated with early IFN-γ-producing CD8$^+$ T cell responses, while late recovery involved a network of humoral (Abs) and cellular (CD8$^+$, CD4$^+$, NK) responses[12]. Here, Flu+ patients' PBMCs were incubated with live seasonal H1N1, H3N2, B/YAM and B/VIC viruses to measure influenza-specific innate (NK, γδ, CD161$^+$TRAV1-2$^+$ or MAIT cells) and adaptive (CD4$^+$ and CD8$^+$ T cells) immune responses elicited via IFN-γ production after 18 hrs (**Fig. 4a,b, Supplementary Fig. 5a**). Kinetics of influenza-specific IFN-γ-producing cells across days after disease onset showed low numbers of IFN-γ-producing populations across all cell subsets at patients' admission. These however increased over the course of infection, before stabilizing at convalescence (**Fig. 4c**). Despite lymphopenia, a fixed number of cells were added to the assay, and therefore the ability of adaptive CD8$^+$ and CD4$^+$ T cells to generate IFN-γ-responses, as a frequency per subset, continued to increase during acute infection until ~15 days after disease onset (**Fig. 4d**). Conversely, for innate cells, their ability to produce IFN-γ responses did not change, further suggesting that adaptive T cells can increasingly respond to the virus during acute infection and are the main drivers of early recovery.

Cytolytic potential of MAIT, NK and CD8$^+$ T cells in Flu+ patients

To assess the cytolytic potential within the Flu+ patients' cell subsets, we measured cytotoxic molecules: granzymes (A, B, K and M) and perforin (**Supplementary Fig. 6a**). Overall, MAIT cells had the highest frequency of total cytotoxic molecules expressed, followed by NK cells and CD8$^+$ T cells, with minimal production in CD4$^+$ T cells (**Fig. 4e**). However, for MAIT cells, the Flu+ patients at acute and convalescence exhibited significantly lower levels compared to healthy donors (demographics in **Supplementary Table 4**), but on the contrary for NK cells, possibly suggesting differences in degranulation kinetics. No differences were observed for CD8$^+$ and CD4$^+$ T cell subsets. Individual expression of cytolytic molecules revealed different patterns between cell subsets and cytolytic molecules (**Fig. 4f**). Patient NK cells had significantly higher levels of granzymes (A, B, M) and perforin compared to healthy donors, but significantly lower levels of granzyme K. Patient MAIT cells expressed lower levels of granzyme A compared to healthy donors, while patient MAIT and CD8$^+$ T cells had lower granzyme K and perforin expression. No significant differences were observed between acute and follow-up subsets. Furthermore, co-expression of multiple cytolytic molecules (4+) was significantly reduced in Flu+ patients, both at acute and follow-up, compared to healthy individuals across all cell subsets (NK cells: acute vs healthy p=0.0002, p<0.0001 for all comparisons) (**Fig. 4g**), most likely reflecting their degranulation activities during influenza infection.

Immune dynamics of activated memory influenza-specific CD8$^+$ and CD4$^+$ T cell responses

To dissect epitope-specific CD8$^+$ and CD4$^+$ T cells during acute IAV infection, we performed patient-specific tetramer staining, utilizing an extensive range of peptide/MHC class-I and class-II tetramers covering the most frequent HLA alleles, with an estimated population coverage of 63-100% across all ethnicities (**Fig. 5a, Supplementary Table 5**). Following tetramer-associated magnetic enrichment (TAME), robust tetramer$^+$CD8$^+$ T cell populations were detected for all donors (n=19) and specificities tested directly *ex vivo* (**Fig. 5b,c, Supplementary Fig. 6b,c**), even when using 10-20% less cell numbers generally required for successful detection of antigen-specific CD8$^+$ T cells in healthy donors[34-36]. In 17 patients, tetramer$^+$CD8$^+$ T cell populations were detected at all the timepoints, while two patients had tetramer$^+$CD8$^+$ T cells directed towards the subdominant B7-NP epitope detectable only at follow-up. For comparison, A2-M1-tetramer$^+$CD8$^+$ T cells were also measured in Flu- patients (n=4/4 detected) (**Fig. 5d**). Apart from CD8$^+$ T cells, we also identified influenza-specific CD4$^+$ T cells in 5/5 H3N2-infected patients with either HLA-DR*01:01-, DR*04:01- or DR*11:01-

HA-tetramers (**Fig. 5e,f**), despite ~10-fold lower numbers of antigen-specific $CD4^+$ T cells *ex vivo*. DR*15:02-HA tetramers were also tested but yielded no specific cells in 2/2 patients.

Overall, tetramer precursor frequencies (where 10^{-3} denotes 1 per 1,000 cells or 1e-3), were stable across timepoints, with no significant differences observed between acute and follow-up (**Fig. 5f**). Pooled $tetramer^+CD8^+$ T cell precursor frequencies in Flu+ patients (mean±SD, range: 2.62e-4±6.37e-4, 8.07e-7 to 3.56e-3) and Flu- patients (7.00e-5±8.11e-5, 8.38e-6 to 2.65e-4) were significantly higher 79-fold ($p<0.0001$) and 21-fold ($p=0.0026$), respectively, than pooled $tetramer^+CD4^+$ T cells (3.30e-6±3.20e-6, 6.19e-7 to 1.17e-5) (**Supplementary Fig. 6d**). Frequencies of pooled $tetramer^+CD8^+$ T cells were similar between Flu+ and Flu- patients and fell within the ranges we described previously for HLA-$A2^+$ H7N9-Flu+ patients[37,38].

Although the frequency of $tetramer^+CD8^+$ T cells were similar between acute and follow-up timepoints in Flu+ patients, and Flu+ versus Flu- patients, the activation phenotypes markedly differed. Based on four activation markers expressed (CD38, HLA-DR, PD-1 and CD71), higher levels of activation were detected at the acute timepoint compared to follow-up (**Fig. 5g, Supplementary Fig. 6e**). Notably, in Flu+ patients, expression of two or more activation markers was most evident between days 6-10 of disease onset for A2-$M1^+CD8^+$ T cells, which was in stark contrast to the mainly single-PD-1 expressing or non-activated phenotypes exhibited among the Flu+ follow-up samples, Flu- patients (**Fig. 5h**), and the parent $CD8^+$ T cell populations. High levels of activation at acute compared to follow-up samples were clearly observed across all $tetramer^+CD8^+$ T cell specificities and, despite limited numbers, in $tetramer^+CD4^+$ T cells when compared to parental $CD8^+$ and $CD4^+$ T cell populations (**Fig. 5i, Supplementary Fig. 7**).

Similarly, analysis of CD27/CD45RA/CD95 phenotypes showed significant differences in the activation of $tetramer^+$ $CD8^+$ and $CD4^+$ T cells in Flu+ patients when compared to the parental $CD8^+$ and $CD4^+$ T cell populations at acute and follow-up timepoints. In general, among Flu+ patients, $tetramer^+CD8^+$ T cells consisted of central memory-like (Tcm, $CD27^+CD45RA^-$) and, to a lesser extent, effector memory-like (Tem, $CD27^-CD45RA^-$) phenotypes, while $tetramer^+CD4^+$ T cells were predominantly of Tcm-like cells. (**Fig. 5j, Supplementary Fig. 6f**). These proportions remained stable across timepoints but were significantly enriched in Tcm compared to the overall $CD4^+$ and $CD8^+$ T cell populations, respectively.

Overall, we show an extensive breadth of highly activated, non-cultured, *ex vivo* influenza-specific memory $CD4^+$ and $CD8^+$ T cells detected during acute IAV infection, which were still present in a less activated state following recovery.

Immune correlates of influenza severity

We also probed clinical, genetic and immune correlates of influenza severity and patients' recovery. We found no significant associations between influenza disease severity (SOFA scores 0-6, clinical presentation: ILI and/or pneumonia), clinical parameters (age, sex, influenza strain, days of disease onset, days in hospital, risk factors and vaccination status) and genetic host factors (IFITM3 rs34481144 SNP alleles). This might be as the majority of hospitalized DISI patients were already in high-risk groups based on their co-morbidities/risk factors (86% Flu+, 70% Flu-), including chronic respiratory disease (61% Flu+, 40% Flu-). Furthermore, patients infected with seasonal influenza viruses experienced less severe disease, with short hospital stays, no requirements for mechanical ventilation, and only one patient requiring ICU for one day, in contrast to the more severe avian H7N9-infected patients[18].

To investigate any potential links between the overall breadth of immune responses in human influenza disease, including cytokines, antibodies, ASCs, activated cTfh1s, IFN-γ-producing innate (NK, γδT, MAIT cells) and adaptive ($CD4^+$ and $CD8^+$ T cells) immune cells, and key clinical/genetic parameters and SOFA scores as a measure for disease severity, we generated heat maps with all of the above mentioned parameters. Unsupervised heat maps of acute and convalescent timepoints were generated for both Flu+ (**Fig. 6a,b, Supplementary Fig. 8a,b**) and Flu- groups, as well as the entire cohort (**Supplementary Fig. 8c-e**). For Flu+ at

the acute timepoints, regions of relatively lower cytokine levels of IL-6, MIP-1α, IL-8, MIP-1β, MCP-1, were linked to higher levels of functional IFN-γ-producing immune cells, ASCs and activated cTfh1s (**Fig. 6a**). As shown in **Fig. 1j**, these cytokines were strongly positively correlated to each other. At convalescence, lower cytokine regions were linked to higher IFN-γ-producing immune cells, but not ASCs or activated cTfh1 cells, which peaked during acute infection (**Fig. 6b**). In both acute and convalescent phases, reciprocal regions of higher cytokines levels and lower IFN-γ-producing immune cells (and lower ASCs and activated cTfh1 cells for acute) were observed. However, these observed regions were not defined specifically by SOFA scores or other clinical/genetic parameters.

Based on the functional implications of IFN-γ-producing cells detected here and our previous H7N9 study[12], we analyzed specifically the numbers of IFN-γ-producing cells across acute (V1) and convalescent timepoints (F_{up}) as a function of patients' disease severity via binned SOFA scores due to unequal numbers of SOFA scores across the cohort, skewing towards low (0-1) SOFA scores, classifying the least severe. At the earliest acute timepoint (V1), decreases in innate IFN-γ-producing γδT and MAIT cells were significantly associated with more severe patients with higher SOFA scores (2-6) (**Fig. 6c**), but not for NK cells, $CD4^+$ and $CD8^+$ T cells. In contrast, at convalescence, lower adaptive IFN-γ-producing $CD4^+$ and $CD8^+$ T cell responses were associated with higher severity (**Fig. 6c**). These results indicated that early influenza-specific NK, $CD4^+$ and $CD8^+$ T cell responses were important in driving patients' recovery from influenza disease, and less severe patients had more robust responses at convalescence, while deficiencies in early innate γδT and MAIT cell responses impacted disease severity.

Discussion

We studied longitudinal samples obtained from patients hospitalized with influenza disease to determine how innate and adaptive immune cellular responses work together to resolve human influenza disease. Influenza susceptibility was associated with high co-morbidities, including people with chronic respiratory disease and immunosuppressed, lower antibody responses and lower rates of vaccination in our cohort. Influenza infection was associated with positively correlated clusters of IL6/IL-8/MIP-1α/MIP-1β cytokines. Antibody responses were low at hospitalization but increased against current and older strains at convalescent phase. The kinetics of activated cTfh-type 1 cells correlated with ASCs and influenza-specific memory B-cell responses, which differed to vaccination-induced B-cell responses. While IFN-γ-producing innate cell responses were unchanged, influenza-specific $CD4^+$ and $CD8^+$ T cell responses increased early from disease onset and tetramer$^+$ $CD4^+$ and $CD8^+$ T cells were highly activated. Collectively, these adaptive cellular mechanisms of cTfh cells, ASCs, influenza-specific B cells and T cells all preceded patients' recovery, similarly to that recently detailed in our COVID-19 case report[39].

Similarly broad and early immunologic analyses of matched hospitalized ILI controls and follow-up samples for both Flu+ and Flu- patients after ~30 days post-discharge have not previously been reported. Our work expands substantially on the SHIVERS study, which included follow-up sampling with blood samples collected from mild non-hospitalized and severe hospitalized influenza-infected patients at the acute phase and at 2 weeks post-enrolment during the 2013 New Zealand winter seasons (Aug-Oct)[26]. The SHIVERS cohort was similar to DISI, enrolling 27 hospitalized patients predominantly infected with a H3N2 virus (83%) and 76% with an underlying condition. However, our study differed from the SHIVERS study by the more rapid enrollment following symptom onset (DISI: 4.5±4.4 days (mean±SD) compared to SHIVERS:10.7±4.8 days) and our patients were hospitalized for longer (DISI median of 4 days (range 1-38 days) compared to SHIVERS median of 2 days (1-10 days). Rapid recruitment and longer hospitalization with serial sampling enabled the capture of integral immune response kinetics very early during the first week of infection, at a time critical for determining patient outcome.

Our cytokine analyses showed that inflammatory cytokines IL-6, IL-8, MIP-1α and MIP-1β were strongly positively correlated with each other, after adjusting for age and the sampling days from disease onset, and supports previous studies on their collective role as biomarkers for influenza severity[18-21]. These cytokine correlations were still robust following recovery at the convalescenct phase compared to other cytokines that were only correlated with each other during acute infection. Furthermore, lower expression of IL-6, IL-8, MIP-1α and MIP-1β were associated with higher IFN-γ-producing immune cells following influenza virus infection assay, as well as ASCs and activated cTfh1 cells, and vice versa.

For antibody responses, HAI antibody titres were lower in Flu+ patients during acute infection compared to Flu- patients and healthy controls, but increased significantly following recovery against the infected strain and previous strains from the same subtype. It is unclear whether the SHIVERS study compared antibody responses between acute versus convalescent phase within mild non-hospitalized and severe hospitalized patient groups, although they did not observe any differences when comparing antibody responses of mild versus severe groups at both acute and convalescent timepoints[26]. Given that we observed back-boosting of cross-reactive antibody responses post-infection at the follow-up timepoint, we postulate that having a natural influenza virus infection, compared to a vaccine-induced response, elicits more effective cross-reactive antibody responses post viral clearance warranting further investigations. Furthermore, acute GMT antibody titres were all below 40 and lower than the Flu- group suggesting that these antibody levels were not protective prior to infection. These findings provide a strong argument for influenza vaccination since the Flu+ group had lower vaccine coverage (48%) than the Flu- group (65%) and supports WHO's guideline of 40 being the 50% protective cut-off which has been controversial. Influenza vaccination is of utmost importance in this cohort given that 86% of Flu+ patients had a significant risk factor for severe influenza disease and 71% of those having a chronic respiratory disease.

We have recently performed a comprehensive study to measure influenza-specific B and T cell responses following seasonal IIV in healthy individuals[4]. Vaccine-induced antibody responses positively correlated with increases in ASCs, influenza-specific memory B cells and a subset of activated cTfh cells. Similarly, during acute influenza disease, we show prominent activation of cTfh1 cells, which correlated with ASC responses and memory influenza-specific B cells. In contrast, numbers of cTfh1 did not correlate with antibody titres at acute, follow-up or fold-change titres. Only ASC numbers positively correlated with higher acute antibody titres of 40 and above, again supporting a cut-off titre of 40 as a measure of protection. The role of cTfh cells as surrogates to germinal center Tfh cells have been described during dengue infection[40] and very recently by our group in a COVID-19 patient[39]. However, to the best of our knowledge, there have been no previous reports on human cTfh cells following natural influenza virus infection.

Interestingly, phenotypic analysis of the memory influenza-specific B cell response showed contrasting profiles induced by infection versus vaccination. During acute infection, influenza-specific B cells were of an activated-memory phenotype comprising IgG and IgA isotypes but were predominantly a resting-memory IgG^+ population at convalescence. Conversely, IIV induced an expansion of activated-memory influenza-specific B cells but there were no changes in the isotype distribution which were predominantly IgG^+ B cells, given that the influenza vaccine is not delivered to a mucosal site. IgA^+ memory B cells are able to localize in the blood and mucosal sites of inflammation such as the respiratory tract during influenza virus infection to provide a rapid immune response, while IgG^+ memory B cells generally circulate throughout the body[45]. Therefore, in accordance with our earlier antibody findings, we suggest that future B cell-based influenza vaccines promoting cross-reactive B cell responses encompassing both activated-memory IgA^+ and IgG^+ subclasses may provide further protection at the site of infection.

Our study utilized a whole live virus assay to measure the kinetics of influenza-specific responses in NK cells, γδ T cells and $CD161^+TRAV1\text{-}2^+$ MAIT cells (innate-like), and $CD8^+$ and $CD4^+$ T cells (adaptive). We observed robust and increasing proportions of adaptive $CD8^+$ and $CD4^+$ T cell responses within the first 2 weeks of infection, despite the patients' overall

lymphphopenic state, illustrating the ability of these cell types to drive patient recovery. In contrast, innate lymphocytes did not increase in their ability to respond to influenza virus infection by cytokine production, and lower IFN-γ-producing γδ T cells and MAIT cells were significantly associated with higher disease severity based on SOFA scores at the earliest V1 timepoint. Similarly, we previously showed the robustness of the adaptive $CD8^+$ and $CD4^+$ T cell immune response in driving recovery from severe H7N9 disease[12]. These findings have important implications for future influenza vaccines because, apart from the $CD4^+$ T cell help compartment, IIV fails to induce $CD8^+$ T cell responses nor any innate responses from NK cells, γδ T cells and MAIT cells, as we previously reported[4].

We probed influenza-specific T cells *ex vivo* using a range of peptide/MHC class I and class II tetramers covering the most frequent HLA alleles with an estimated population coverage of 63-100% across all ethnicities. $Tetramer^+$ $CD8^+$ and $CD4^+$ T cells were highly activated at acute timepoints, compared to a less activated profile at follow-up, and mainly expressed combinations of PD-1 with CD38 and CD71, and HLA-DR to a lesser extent. In contrast to severe H7N9 influenza[13], Ebola[46] and COVID-19 disease[39], with prominent $CD38^+HLA\text{-}DR^+$ populations in the total CD8/CD4 compartments, we did not observe marked populations of $CD38^+HLA\text{-}DR^+$ T cells in either $tetramer^+$ or parent populations, perhaps reflecting a less severe cohort of diseased patients in our DISI study. Nonetheless, we provide acute and convalescent populations of rare $HA_{306\text{-}318}$-specific $CD4^+$ T cells in H3N2-infected patients that were HLA-DR*01:01$^+$ (*n*=3), HLA-DR*04:01$^+$ (*n*=1) or HLA-DR*11:01$^+$ (*n*=1), which complements other studies assessing cells in HLA-DR*04:01$^+$ healthy donors and rheumatoid arthritis patients following influenza vaccination[47,48]. Therefore, our results represent the broadest array of influenza-specific $tetramer^+$ T cell responses during acute influenza infection, providing essential tools for future T cell-immune monitoring of newly-emerging influenza viruses.

Tracking antibody, B and T cell responses (and other immune mediators) may be predictive of patients' severity or recovery from influenza virus infections that require hospitalization. Our current analyses of immunological and virological parameters within a clinical hospital framework provide a unique and key dataset on the mechanisms underpinning influenza severity and susceptibility in the human population. Furthermore, these efforts represent a substantial progression to elucidate the host immune responses underlying the recovery from this acute disease as well as other infectious diseases such as COVID-19[39].

Online Methods

Study participants and design

The Dissection of Influenza-Specific Immunity (DISI) cohort enrolled consenting adult patients admitted to The Alfred hospital during the 2014-2017 peak influenza seasons with influenza-like illness. Influenza-positive patients were PCR-confirmed (*n*=44), while ILI influenza-negative patients with other respiratory diseases were treated as negative controls (*n*=20). Bloods were collected within 24-72 hours of hospital admission (Visit 1, V1), every 2-5 days until discharge (V2, V3, V4 etc), then followed up approximately 30 days later. Nasal swabs were collected at V1 and V2 timepoints while in hospital. Clinical data collection included vaccination status, sequential (sepsis-related) organ failure assessment (SOFA) score[28] as a measure of disease severity, and any significant risk factors (**Supplementary Tables 1 and 2**).

The H7N9-infected hospitalized patient cohort (*n*=18) has previously been described[18]. Healthy adults vaccinated in 2015 (TIV, *n*=16) and 2016 (QIV, *n*=26) have previously been described in detail[4], where blood samples were collected prior to vaccination (day -1 or 0) and on days 7, 14 and 28 following vaccination. Healthy blood donors were recruited from The University of Melbourne and Deepdene Surgery. Buffy packs were sourced from Australian Red Cross Lifeblood, respectively (**Supplementary Table 4**).

Human experimental work was conducted according to the Declaration of Helsinki Principles and according to the Australian National Health and Medical Research Council Code of Practice. All participants provided written informed consent prior to the study. The study was

approved by the Alfred Hospital (ID #280/14) and University of Melbourne (ID #1442952.1 and #1443389.4) Human Research Ethics Committees. Up to 40 mls of DISI patient blood was collected in sodium heparin tubes (including 1 serum tube) and processed within 24 hours. Up to 60 mls was collected from healthy donors and ~50-60 ml for buffy packs. PBMCs were isolated by Ficoll-Paque (GE Healthcare, Uppsala, Sweden) density-gradient centrifugation and cryopreserved. DNA was extracted from the granulocyte layer using a QIAamp DNA Mini Kit (Qiagen, Hilden, Germany) and sent to the Victorian Transplantation and Immunogenetics Service (Australian Red Cross Lifeblood, West Melbourne, Victoria, Australia) for HLA class I and class II molecular typing using the Luminex platform and microsphere technology (One Lambda, Canoga Park, CA, USA), with LABType SSO HLA typing kits (One Lambda). Nasal swab samples were kept cold during transport and stored at -80°C within 4 hours.

In cases where fewer than the total number of donors were analyzed (**Supplementary Table 6**), DISI patients were selected for influenza-specific cellular assays based on their influenza status and remaining sample availability, such as the class I and II TAME experiments which were carried out on IAV^+ patients and relied on HLA type and tetramer availability. HIV-positive patients (*n*=5, **Supplementary Table 2**) were not included in such experiments to fulfil biocontainment regulations. No other blinding or randomization protocols were applied and no outliers (i.e. the two death patients) were excluded.

IFITM3 SNP analysis

Amplification of *exon 1* rs12252 region was performed by PCR on genomic DNA using forward (5′-GGAAACTGTTGAGAAACCGAA-3′) and reverse (5′-CATACGCACCTTCACGGAGT-3′) primers, as previously described[49]. Amplification of the rs34481144 promotor region was performed using forward (5′-GGAAACTGTTGAGAAACCGAA-3′) and reverse (5′-CATACGCACCTTCACGGAGT-3′) primers, as described[17].

Cytokine analysis

Patient's sera or plasma was diluted 1:4 for performing cytokine bead assay (CBA) using the Human CBA Kit (BD Biosciences, San Jose, California, USA), according to manufacturer's instructions. Capture beads included IL-2, IL-4, IL-6, IL-8, IL-10, IL-12p70, IL-17A, IL-1β, IFN-α, MIP-1α, MIP-1β, MCP-1, CD178/FasL, granzyme B, RANTES, TNF and IFN-γ. Samples were also diluted 1:100 for RANTES. A limited panel of cytokines for H7N9 patients have already been described[18].

Viral sequencing

Viral isolates from nasal swabs were sequenced for HA using standard Sanger sequencing methods. HA phylogenetic neighbour-joining trees were produced using Geneious 9.0.4 software. Sequences are on the GISAID database with ID numbers of EPI_ISL_312219-312221, 312673-312674.

Viruses

Influenza A (A/H1N1/California/7/2009, A/H3N2/Switzerland/9715293/2013 and H3N2/Hong Kong/4801/2014) and B (B/YAM/Phuket/3073/2013 and B/VIC/Brisbane/60/2008) viruses were grown in 10-day old embryonated chicken eggs at 33°C for 72 hours. Allantoic fluid was harvested and titrated using standard plaque assays in MDCK cells for use in the influenza infection assays. Other viruses (**Supplementary Table 3**) were sourced from the WHO Collaborating Centre for Reference and Research on Influenza (Melbourne, Australia).

Hemagglutination inhibition assay

RDE-treated sera or plasma samples were assessed for antibody titres against a panel of influenza viruses (**Supplementary Table 3**) using standard HAI assays with 1% turkey red blood cells (H1N1 and IBV) or 1% guinea pig red blood cells in the presence of oseltamivir (H3N2), according to WHO guidelines. HAI titres were reported as the reciprocal of the highest

dilution of serum where hemagglutination was completely inhibited, then divided by 10 and $\log_2$-transformed.

Flow cytometry

Fresh whole blood was used to measure absolute cell numbers using BD TruCount tubes and BD MultiTest (CD3 FITC/CD16+CD56 PE/CD45 PerCP/CD19 APC, #340500) according to manufacturer's instructions (BD Biosciences), as well as Tfh and ASC populations as described[4]. Thawed PBMCs from Flu+ patients were stained with recombinant (r) HA probes from H1 (California/7/2009), H3 (Switzerland/9715293/2013 or Hong Kong/4801/2014) and B strains (Phuket/3073/2013 or Brisbane/60/2008)[4,32], as described, except anti-IgA was not included in rH1 and rH3 probe panels. PBMCs stained with other antibody panels are indicated under specific assays. TruCount/MultiTest samples were acquired on a BD CantoII. All other samples were acquired on a BD LSRII Fortessa. Flow cytometry data were analyzed using FlowJo v10 software.

Influenza virus infection assay

Thawed PBMCs (<1.5e6) from DISI Flu+ patients were cultured overnight at 37°C/5% CO_2 with their cognate live egg-grown virus (MOI=4), essentially as described[4,12], for a total of 22 hours before cells were harvested, then cell surface and intracellularly stained with Panel 1a or 1b (**Supplementary Table 7**) using the BD Cytofix/Cytoperm Kit according to manufacturer's instructions. A no virus culture was included as a background staining control, which was subtracted from the virus culture.

Tetramer-associated magnetic enrichment (TAME)

TAME was performed on thawed PBMCs (3-38e6) for the detection of influenza-specific $CD4^+$ and $CD8^+$ T cells, as described[36,37]. Peptide/MHC class I and class II monomers (**Fig. 5a**) were generated in-house[50,51], before 8:1 molar ratio conjugation with either PE-streptavidin (SA) or APC-SA (BD Biosciences) to form tetramers. Briefly, cells were stained (1:100-200 dilution) with PE- (A2-M1, B7-NP, B8-NPs, B18-NP and B35-NPs) or APC-labelled (A1-NPs, A2-M1, A24-PB1, A68-NP, B57-NP and DR1/4/11-HAs) tetramers for 1 hour at room temperature before dual-magnetic enrichment with anti-PE and anti-APC MicroBeads (Miltenyi Biotec, Bergisch Galdbach Germany) as described[36,38]. Tetramers restricted to the same HLA were added together at the same dilution. Unenriched, enriched and flow-through fractions were cell surface stained with Panel 2a (Flu+) or 2b (Flu-, follow-up samples only) (**Supplementary Table 7**), fixed with 1% PFA, then acquired by flow cytometry. Panel 2b samples were fixed and permeabilized using the eBioscience™ Foxp3/Transcription Factor Staining Buffer Set (Thermo Fisher Scientific, Carlsbad, CA, USA). Samples with cell events just below 10, especially for $tetramer^+CD4^+$ T cells, were not further characterized phenotypically using these staining panels.

Expression of cytolyic molecules

Flow-through fractions of DISI patients following TAME or thawed PBMCs from healthy donors (**Supplementary Table 4**) were stained with Panel 3 (**Supplementary Table 7**) for measuring granzymes (A, B, K and M) and perforin using the Foxp3/Transcription Factor Staining Buffer Set.

Statistical analyses

Statistical significance was assessed using GraphPad Prism v8 software unless stated otherwise. Mann-Whitney (unpaired) and Wilcoxin (paired) tests were two-tailed. Friedman (matched) and Kruskal-Wallis (unmatched) tests were used to compare more than two groups. Tukey's multiple comparison test compared row means between more than two groups. Partial correlation plots (**Fig. 1j**) showing significant (FDR-adjusted p-value <0.05) coloured squares were partialed to account for the variance caused by $\log_{10}$(age) and the sampling days after disease onset. To build antibody landscapes (**Fig. 2f**), local regression (LOESS) was applied in R 3.5.3[52]. LOESS with 95% confidence intervals was also used to plot Fig. 3c, 4c and 4d. Linear

relationships between day of sample and percent of IFN-γ producing cells were assessed with ordinary least squares (lm function) in R with 95% confidence intervals shaded in grey and correlation coefficients (r^2) reported in Fig 4d. Correlations (**Fig. 3f,g, Supplementary Fig. 4**) were assessed using Spearman's correlation coefficient (r_s). Polyfunctionality pie charts (**Fig. 4g**) were generated using Pestle v1.8 and Spice v5 software[53] and *p*-values were calculated using Permutation Test. *P*-values lower than 0.05 were considered statistically significant and exact *p*-values are shown in the figure. All statistical tests are indicated in the figure legends.

Data availability

The data that support the findings of this study are available from the corresponding author upon request.

References

1. G. B. D. Influenza Collaborators. Mortality, morbidity, and hospitalisations due to influenza lower respiratory tract infections, 2017: an analysis for the Global Burden of Disease Study 2017. *Lancet Respir Med* **7**, 69-89 (2019).
2. Iuliano, A.D., *et al.* Estimates of global seasonal influenza-associated respiratory mortality: a modelling study. *Lancet* **391**, 1285-1300 (2018).
3. Krammer, F., *et al.* Influenza. *Nat Rev Dis Primers* **4**, 3 (2018).
4. Koutsakos, M., *et al.* Circulating TFH cells, serological memory, and tissue compartmentalization shape human influenza-specific B cell immunity. *Sci Transl Med* **10**(2018).
5. McMichael, A.J., Gotch, F.M., Noble, G.R. & Beare, P.A. Cytotoxic T-cell immunity to influenza. *N Engl J Med* **309**, 13-17 (1983).
6. Epstein, S.L. Prior H1N1 influenza infection and susceptibility of Cleveland Family Study participants during the H2N2 pandemic of 1957: an experiment of nature. *J Infect Dis* **193**, 49-53 (2006).
7. Kreijtz, J.H., *et al.* Cross-recognition of avian H5N1 influenza virus by human cytotoxic T-lymphocyte populations directed to human influenza A virus. *J Virol* **82**, 5161-5166 (2008).
8. Sridhar, S., *et al.* Cellular immune correlates of protection against symptomatic pandemic influenza. *Nat Med* **19**, 1305-1312 (2013).
9. Wilkinson, T.M., *et al.* Preexisting influenza-specific CD4+ T cells correlate with disease protection against influenza challenge in humans. *Nat Med* **18**, 274-280 (2012).
10. Zhao, Y., *et al.* High levels of virus-specific CD4+ T cells predict severe pandemic influenza A virus infection. *Am J Respir Crit Care Med* **186**, 1292-1297 (2012).
11. Hayward, A.C., *et al.* Natural T Cell-mediated Protection against Seasonal and Pandemic Influenza. Results of the Flu Watch Cohort Study. *Am J Respir Crit Care Med* **191**, 1422-1431 (2015).
12. Wang, Z., *et al.* Recovery from severe H7N9 disease is associated with diverse response mechanisms dominated by CD8(+) T cells. *Nat Commun* **6**, 6833 (2015).
13. Wang, Z., *et al.* Clonally diverse CD38(+)HLA-DR(+)CD8(+) T cells persist during fatal H7N9 disease. *Nat Commun* **9**, 824 (2018).
14. van de Sandt, C.E., *et al.* Human cytotoxic T lymphocytes directed to seasonal influenza A viruses cross-react with the newly emerging H7N9 virus. *J Virol* **88**, 1684-1693 (2014).
15. Hertz, T., *et al.* HLA targeting efficiency correlates with human T-cell response magnitude and with mortality from influenza A infection. *Proc Natl Acad Sci U S A* **110**, 13492-13497 (2013).

16. Falfan-Valencia, R., *et al.* An Increased Frequency in HLA Class I Alleles and Haplotypes Suggests Genetic Susceptibility to Influenza A (H1N1) 2009 Pandemic: A Case-Control Study. *J Immunol Res* **2018**, 3174868 (2018).
17. Allen, E.K., *et al.* SNP-mediated disruption of CTCF binding at the IFITM3 promoter is associated with risk of severe influenza in humans. *Nat Med* **23**, 975-983 (2017).
18. Wang, Z., *et al.* Early hypercytokinemia is associated with interferon-induced transmembrane protein-3 dysfunction and predictive of fatal H7N9 infection. *Proc Natl Acad Sci U S A* **111**, 769-774 (2014).
19. Lee, N., *et al.* Cytokine response patterns in severe pandemic 2009 H1N1 and seasonal influenza among hospitalized adults. *PLoS One* **6**, e26050 (2011).
20. Oshansky, C.M., *et al.* Mucosal immune responses predict clinical outcomes during influenza infection independently of age and viral load. *Am J Respir Crit Care Med* **189**, 449-462 (2014).
21. Hall, M.W., *et al.* Innate immune function and mortality in critically ill children with influenza: a multicenter study. *Crit Care Med* **41**, 224-236 (2013).
22. Valkenburg, S.A., *et al.* The Hurdles From Bench to Bedside in the Realization and Implementation of a Universal Influenza Vaccine. *Front Immunol* **9**, 1479 (2018).
23. Dunning, J., *et al.* Progression of whole-blood transcriptional signatures from interferon-induced to neutrophil-associated patterns in severe influenza. *Nat Immunol* **19**, 625-635 (2018).
24. Fox, A., *et al.* Severe pandemic H1N1 2009 infection is associated with transient NK and T deficiency and aberrant CD8 responses. *PLoS One* **7**, e31535 (2012).
25. Diao, H., *et al.* Severe H7N9 infection is associated with decreased antigen-presenting capacity of CD14+ cells. *PLoS One* **9**, e92823 (2014).
26. Wong, S.S., *et al.* Severe Influenza Is Characterized by Prolonged Immune Activation: Results From the SHIVERS Cohort Study. *J Infect Dis* **217**, 245-256 (2018).
27. Quinones-Parra, S., *et al.* Preexisting CD8+ T-cell immunity to the H7N9 influenza A virus varies across ethnicities. *Proc Natl Acad Sci U S A* **111**, 1049-1054 (2014).
28. Singer, M., *et al.* The Third International Consensus Definitions for Sepsis and Septic Shock (Sepsis-3). *JAMA* **315**, 801-810 (2016).
29. Fonville, J.M., *et al.* Antibody landscapes after influenza virus infection or vaccination. *Science* **346**, 996-1000 (2014).
30. Crotty, S. Follicular helper CD4 T cells (TFH). *Annu Rev Immunol* **29**, 621-663 (2011).
31. Bentebibel, S.E., *et al.* Induction of ICOS+CXCR3+CXCR5+ TH cells correlates with antibody responses to influenza vaccination. *Sci Transl Med* **5**, 176ra132 (2013).
32. Liu, Y., *et al.* Cross-lineage protection by human antibodies binding the influenza B hemagglutinin. *Nat Commun* **10**, 324 (2019).
33. Wheatley, A.K., Kristensen, A.B., Lay, W.N. & Kent, S.J. HIV-dependent depletion of influenza-specific memory B cells impacts B cell responsiveness to seasonal influenza immunisation. *Sci Rep* **6**, 26478 (2016).
34. Nguyen, T.H., *et al.* Maintenance of the EBV-specific CD8(+) TCRalphabeta repertoire in immunosuppressed lung transplant recipients. *Immunol Cell Biol* **95**, 77-86 (2017).
35. Nguyen, T.H., *et al.* Understanding CD8(+) T-cell responses toward the native and alternate HLA-A*02:01-restricted WT1 epitope. *Clin Transl Immunology* **6**, e134 (2017).
36. Nguyen, T.H.O., *et al.* Perturbed CD8(+) T cell immunity across universal influenza epitopes in the elderly. *J Leukoc Biol* **103**, 321-339 (2018).
37. Koutsakos, M., *et al.* Human CD8(+) T cell cross-reactivity across influenza A, B and C viruses. *Nat Immunol* **20**, 613-625 (2019).
38. Sant, S., *et al.* Single-Cell Approach to Influenza-Specific CD8(+) T Cell Receptor Repertoires Across Different Age Groups, Tissues, and Following Influenza Virus Infection. *Front Immunol* **9**, 1453 (2018).
39. Thevarajan, I., *et al.* Breadth of concomitant immune responses prior to patient recovery: a case report of non-severe COVID-19. *Nat Med* **26**, 453-455 (2020).

40. Haltaufderhyde, K., *et al.* Activation of Peripheral T Follicular Helper Cells During Acute Dengue Virus Infection. *J Infect Dis* **218**, 1675-1685 (2018).
41. Leong, Y.A., *et al.* CXCR5(+) follicular cytotoxic T cells control viral infection in B cell follicles. *Nat Immunol* **17**, 1187-1196 (2016).
42. He, R., *et al.* Follicular CXCR5- expressing CD8(+) T cells curtail chronic viral infection. *Nature* **537**, 412-428 (2016).
43. Petrovas, C., *et al.* Follicular CD8 T cells accumulate in HIV infection and can kill infected cells in vitro via bispecific antibodies. *Sci Transl Med* **9**(2017).
44. Mylvaganam, G.H., *et al.* Dynamics of SIV-specific CXCR5+ CD8 T cells during chronic SIV infection. *Proc Natl Acad Sci U S A* **114**, 1976-1981 (2017).
45. Auladell, M., *et al.* Recalling the Future: Immunological Memory Toward Unpredictable Influenza Viruses. *Front Immunol* **10**, 1400 (2019).
46. McElroy, A.K., *et al.* Human Ebola virus infection results in substantial immune activation. *Proc Natl Acad Sci U S A* **112**, 4719-4724 (2015).
47. Uchtenhagen, H., *et al.* Efficient ex vivo analysis of CD4+ T-cell responses using combinatorial HLA class II tetramer staining. *Nat Commun* **7**, 12614 (2016).
48. Herati, R.S., *et al.* Successive annual influenza vaccination induces a recurrent oligoclonotypic memory response in circulating T follicular helper cells. *Sci Immunol* **2**(2017).
49. Clemens, E.B., *et al.* Towards identification of immune and genetic correlates of severe influenza disease in Indigenous Australians. *Immunol Cell Biol* **94**, 367-377 (2016).
50. Gras, S., *et al.* The shaping of T cell receptor recognition by self-tolerance. *Immunity* **30**, 193-203 (2009).
51. Benati, D., *et al.* Public T cell receptors confer high-avidity CD4 responses to HIV controllers. *J Clin Invest* **126**, 2093-2108 (2016).
52. R Core Team. R: A language and environment for statistical computing. R Foundation for Statistical Computing, Vienna, Austria. (2019. http://www.R-project.org/.).
53. Roederer, M., Nozzi, J.L. & Nason, M.C. SPICE: exploration and analysis of post-cytometric complex multivariate datasets. *Cytometry A* **79**, 167-174 (2011).

Acknowledgements

We thank Jill Garlick, Janine Roney, and the research nurses at the Alfred Hospital, Nicola Bird, Kim Harland, Louise Carolan and Bernadette McCudden for their technical assistance. Thank you to Professors David Fairlie and Jim McCluskey for the MR1-5'OP-RU tetramer. We also thank the study participants for providing blood for research purposes.

Funding

The Australian National Health and Medical Research Council (NHMRC) NHMRC Program Grant (1071916) to KK, SJT, NLG, AK, DCJ, LEB, WC supported this work. MK and SN were recipients of Melbourne International Research Scholarship and Melbourne International Fee Remission Scholarship. CES has received funding from the European Union's Horizon 2020 research and innovation program under the Marie Skłodowska-Curie grant agreement No. 792532. EBC is a NHMRC Peter Doherty Fellow. MA and LH are recipients of Melbourne International Research Scholarship and Melbourne International Fee Remission Scholarship. SS was a recipient Victoria India Doctoral Scholarship and Melbourne International Fee Remission Scholarship, University of Melbourne. The Melbourne WHO Collaborating Centre for Reference Research on Influenza is supported by the Australian Government Department of Health. SG is a NHMRC SRF-Level A Fellow. JR is supported by an ARC Laureate fellowship. NLG is supported by a NHMRC Ideas grant, ARC Discovery Project and ARC Future Fellowship. PGT is supported by the St. Jude Center of Excellence for Influenza Research and Surveillance (NIAID Contract HHSN27220140006C), R01 AI 107625, R01AI136514 and ALSAC. ACC is a NHMRC Career Development (level 2) Fellow. KK was supported by a

NHMRC Senior Research Fellowship Level B (#1102792), NHMRC Investigator Grant (#1173871) and the University of Melbourne Dame Kate Campbell Fellowship.

Conflicts of interest

The authors declare no conflict of interest.

Author contributions

KK supervised and lead the study. KK, THON, MK, CES and LL designed the experiments. THON, MK, CES, LL, LG, SS, EBC, MAu, LH, ZW, SN, AF, XX, MAb, KLL and YD performed experiments. THON, MK, CES, JCC, LL, LG, EKA, TB, EBC, MAu, LH, ACH, PGT and KK analyzed data. AKW and SJK provided invaluable rHA probes. SG and JR provided invaluable pMHC-I/II tetramers. JC, JX, TCK and ACC recruited the patient cohorts. KK, ACC, TCK, SJT, PCD, DJ, LEB, NLG and WC provided intellectual input into the study design and data interpretation. THON, PGT, ACC and KK wrote the manuscript. All authors reviewed and approved the manuscript.

Competing interests

All authors declare no competing interests.

Figure legends

Fig. 1. **Clustering analysis of patient clinical information, genetic characteristics and inflammatory cytokines**. **a**, Flow chart of study design. **b**, Frequency of patients infected with seasonal influenza virus strains. *N* values are below for total and for each year. **c**, Age distribution by influenza A (3 unsubtyped, 7 H1N1, 24 H3N2), influenza B (3 unsubtyped, 4 YAM, 3 VIC) and influenza-negative (Non-flu, Flu-) patients (n=20). Virus strain colours match those in (**b**). **d**, Days in hospital for DISI cohort and H7N9 cohort. **c**,**d**, Bars indicate the median and IQR, statistical significance (p<0.05) was determined using the Kruskal-Wallis test. **e**, Frequency of universal versus risk HLA alleles between influenza-positive (Flu+) and Flu- patients. **f**,**g**, Pie charts of IFITM3 SNP allele genotyping at positions rs12252 and rs34481144, respectively (risk allele in black). **h**, Box plots of rs34481144 alleles against SOFA scores showing median, IQR and whiskers extending to the largest or smallest values no further than 1.5 times the IQR. **i**, Representative serum levels and distribution of pro-inflammatory cytokines in patients, measured within the first 2-3 days of hospital admission (Visit 1, V1), with varying disease severity. **j**, Partial correlation plots showing the degree of correlation between every chemokine/cytokine pair in Flu+ patients at V1 and F_{up}. The colour corresponds to the correlation coefficient and the size of the colored squares correspond to the FDR-adjusted p-value. Correlations that are not significant (p>0.05) result in white boxes.

Fig. 2. Viral analysis and antibody responses. **a**, H3N2 phylogenetic tree of HA amino acid sequences from previous WHO reference strains in black, influenza vaccine strains in red and sequences isolated from the nasal swab of 12 H3N2-infected patients in blue. Patient number is followed by the year of recruitment, yes (Y) or no (N) for prior vaccination in the year of infection, and "mm*" indicates whether the vaccine was a clade mismatch in that year. Scale bar represents the number of substitutions per site. **b**, Antibody HAI titers of Flu+ patients at acute (V1 or V2) and follow-up timepoints from the relevant infected strain (mean and SD are shown). Statistical significance (p<0.05) was determined using the Mann-Whitney test between acute and follow-up per strain. **c**,**d**, Geometric mean titers (GMT) per strain in Flu+ and Flu- patients at acute and follow-up, and from a healthy vaccinated cohort at days 0 and 28 post-vaccination. **b-d,** Both H1N1 and H3N2 titers are shown for three A/unsubtyped patients and both B/YAM/Phuket/3073/2013 and B/VIC/Brisbane/60/2008 titres are shown for three B/unsubtyped patients (square symbols). **e**, Representative antibody landscapes from a patient infected with H1N1, H3N2, B/YAM or B/VIC virus. Blue shading indicate period of potential exposure based on the year born. **f**, Antibody landscapes of H1N1- and H3N2-infected (n=7 and 23, respectively) and H1N1- and H3N2-non-infected patients (n=45 and 29, respectively). Lines

and shading indicate the GMT and 95% confidence intervals, respectively. Gradient coloured dots indicate individual titres.

Fig. 3. Circulating Tfh cells, ASCs and influenza-specific B cell responses. a, Representative FACS plots of $CD4^+CXCR5^+$ cTfh subsets (cTfh1/2/17) and expression of activation markers PD-1 and ICOS. **b**, Representative FACS plots of $CD19^+CD20^{-/lo}CD27^{++}CD38^{++}$ ASCs and $PD\text{-}1^+ICOS^+$ activated $CXCR3^+CCR6^-$ cTfh1 cells at acute (V1 and V2) and follow-up (F_{up}) timepoints. Days (d) after disease onset are shown in brackets. **c**, Numbers of ASC and cTfh1 cells of Flu+ (red) and Flu- (blue) patients after disease onset. Grey shading represents 95% confidence intervals. **d**, Numbers of the peak ASC responses during acute ILI (Ac_{max}) versus F_{up} in Flu+ (open circles, Ac_{max} n=40, F_{up} n=32) and Flu- patients (grey circles, Ac_{max} n=19, F_{up} n=15). **e**, Peak cTfh responses of different Tfh1/2/17 subsets at Ac_{max} (Flu+ n=40, Flu- n=19) and F_{up} (Flu+ n=32, Flu- n=15) timepoints. **f**, Correlation (Spearman correlation coefficient, r_s) between Ac_{max} ASC and cTfh1 responses and **(g)** Ac_{max} ASC responses with HAI antibody titres of high (HAI≥40) and low responders (HAI<40) during acute infection. **h**, Representative FACS plots of H1-, H3- and B-specific rHA^+ B cells at V1 and F_{up} timepoints (days after disease onset in brackets). **i**, Numbers of total rHA^+ B cells and per H1-, H3- and B-specific rHA^+ B cells at acute (Ac) (n=21) and F_{up} timepoints (n=22). **j**, Representative overlay FACS plots of live total B cells and rHA^+ B cells from IBV-infected patient #29 at F_{up} for phenotype and isotype characterization. **k-m**, Phenotype (top panel) and isotype (bottom panel) distributions of (**k**) total B cells and (**l**) rHA^+ B cells in Flu+ patients at acute (Ac=V1 and V2, V1, V2) and follow-up timepoints in comparison to (**m**) healthy vaccinated controls (n=41) pre-vaccination at baseline (BL) and d7, 14 and 28 post-vaccination. **d,e,i**, Red bars indicate the median and IQR for cell numbers. **k-m**, Bars indicate the mean and SD for frequencies. Statistical significance (p<0.05) was determined using the (**d**) Mann-Whitney test, (**e**) Friedman test and (**k-m**) Tukey's multiple comparison test. Coloured p-values refer to each group legend within the graph.

Fig. 4. Innate and adaptive immune responses in seasonal influenza-infected patients. a-d, Data following influenza virus infection assay. **a**, Representative FACS plots of innate (NK cells, γδ T cells and $CD161^+TRAV1\text{-}2^+$ MAIT cells) and adaptive ($CD4^+$ and $CD8^+$ T cells) immune cell subsets gated on live/$CD14^-$/$CD19^-$ singlet lymphocytes. **b**, Representative FACS plots measuring frequency of infection (intracellular nucleoprotein (NP) staining) and IFN-γ production for each immune cell subset. Infection in PBMCs by intracellular NP-staining showing consistent infectivity rates over time across the donors (**Supplementary Fig. 5b**). MAIT cells were defined as $CD161^+TRAV1\text{-}2^+$ and were validated by the MR1-5'OP-RU-tetramer in 51% of samples (**Supplementary Fig. 5c,d**). **c,d**, Numbers (n=22) and frequencies (n=30) of influenza-specific IFN-γ-production in patients' immune cell subsets as days of disease onset where 95% confidence intervals are shaded in grey. **e-g**, Patient data from PBMCs left over from flow through fraction following TAME. *NK cells were defined by live/$CD14^-$/$CD19^-$/$CD3^-$ cells. ^MAIT cells were defined by the MR1-5-OP-RU-tetramer and anti-TRAV1-2 antibody. **e**, Frequency (mean, SD) of Flu+ patient cells expressing total cytotoxic molecules at acute (includes n=16 at V1 and n=11 at subsequent visits i.e. V2, V3, or V4) and follow-up timepoints (n=19), in comparison to healthy donors (n=20, except for MAIT subset where n=12). **f**, Representative FACS plots of $CD8^+$ T cells from Flu+ patient and individual frequencies (mean, SD) of granzymes (A, B, K and M) and perforin staining for each cell subset. **g**, Pie charts representing the average fractions of cells co-expressing different cytotoxic molecules (slices) and the combinations of granzymes and perforin molecules (arcs). Statistical significance (p<0.05) was determined using (**e,f**) Tukey's multiple comparison and (**g**) Permutation tests.

Fig. 5. Influenza-specific $CD4^+$ and $CD8^+$ T cell responses. a, List of influenza-specific HLA class I (A, B) and class II (DR) tetramers used in the study. **b**,**c**, Concatenated FACS plots of TAME-enriched class I-$tetramer^+$ cells gated on $CD8^+$ T cells from Flu+ patients and (**d**) Flu- patients. Individual tetramer precursor frequencies are shown below for patients in (**b**). **e**,

Concatenated FACS plots of TAME-enriched class II-tetramer$^+$ cells gated on CD4$^+$ T cells from H3N2-infected patients. **f**, Precursor frequencies of tetramer$^+$ cells from Flu+ and Flu- patients at acute (V1, V2, V3 or V4) and follow-up timepoints. **g**, Representative overlay FACS plots of activation markers expressed on TAME-enriched tetramer$^+$ cells compared to their unenriched parent population. **h**, Frequency of A2-M1$^+$CD8$^+$ T cells from individual Flu+ and Flu- patients expressing different combinations of activation markers PD-1, CD38, HLA-DR and CD71, where CD71 was replaced by Ki-67 in the staining panel for Flu- patients. **i**, Overall activation status of TAME-enriched tetramer$^+$ cells compared to their unenriched parent population of CD4$^+$ or CD8$^+$ T cells in Flu+ patients. **j**, T cell differentiation phenotype of TAME-enriched tetramer$^+$ cells in relation to the unenriched parent population of CD4$^+$ or CD8$^+$ T cells. **i**,**j**, Mean and SD are shown for all acute and follow-up timepoints, except for the acute tetramer$^+$CD4$^+$ group (n=2), which were plotted individually. Statistical significance (p<0.05) was determined using Tukey's multiple comparison test for (**i**) number of activation markers present (0, 1 or 2+) and (**j**) T cell differentiation subsets.

Fig. 6. Analyses of immune responses and clinical and genetic host factors. a,**b**, Unsupervised heatmaps of immune, clinical and genetic parameters in Flu+ patients at **a**, acute and **b**, convalescent timepoints. Interactive heatmaps (.html) are shown in **Supplementary Fig. 8a-e** for Flu+, Flu- and combined datasets. Regions of low (maroon) and high (pink) cytokine clusters are boxed. **c**, Box plots of IFN-γ-producing cells following influenza virus infection assay, at the earliest acute (V1) and convalescent (F_{up}) timepoints as a function of patients' disease severity via binned SOFA scores of 0-1 versus 2-6. Median, IQR and whiskers extending to the largest or smallest values no further than 1.5 times the IQR are shown. Nonparametric Wilcoxon rank sum test with continuity correction was used for comparisons between SOFA categories. Wilcoxon signed rank test (a paired test) was used to compare differences between V1 and F_{up} among the same individuals. Tests were carried out on the actual data, although plots were on a log10+1 scale for ease of visualization.

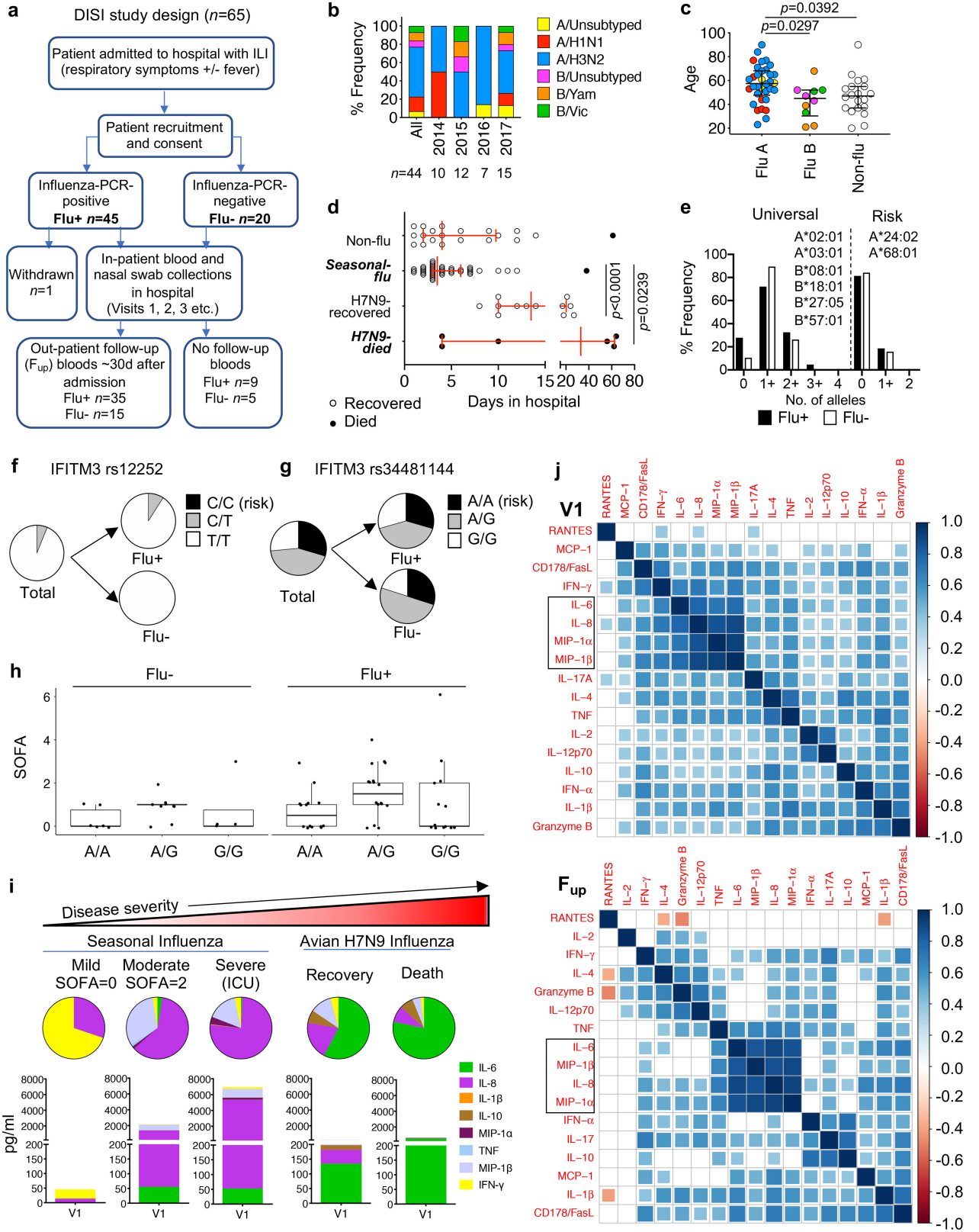

Figure 1 Nguyen *et al*.

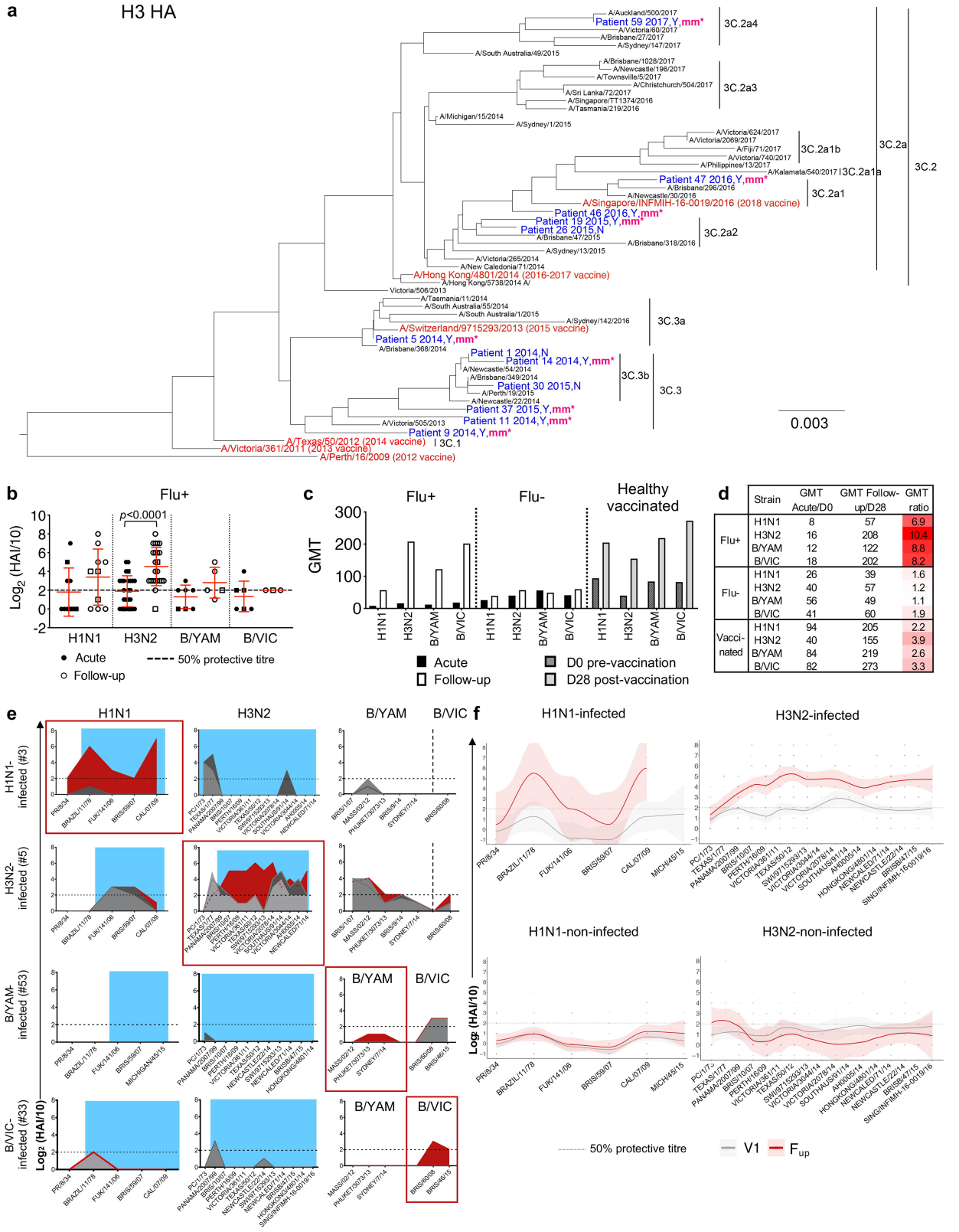

	Strain	GMT Acute/D0	GMT Follow-up/D28	GMT ratio
Flu+	H1N1	8	57	6.9
	H3N2	16	208	10.4
	B/YAM	12	122	8.8
	B/VIC	18	202	8.2
Flu-	H1N1	26	39	1.6
	H3N2	40	57	1.2
	B/YAM	56	49	1.1
	B/VIC	41	60	1.9
Vacci-nated	H1N1	94	205	2.2
	H3N2	40	155	3.9
	B/YAM	84	219	2.6
	B/VIC	82	273	3.3

Figure 2 Nguyen *et al*.

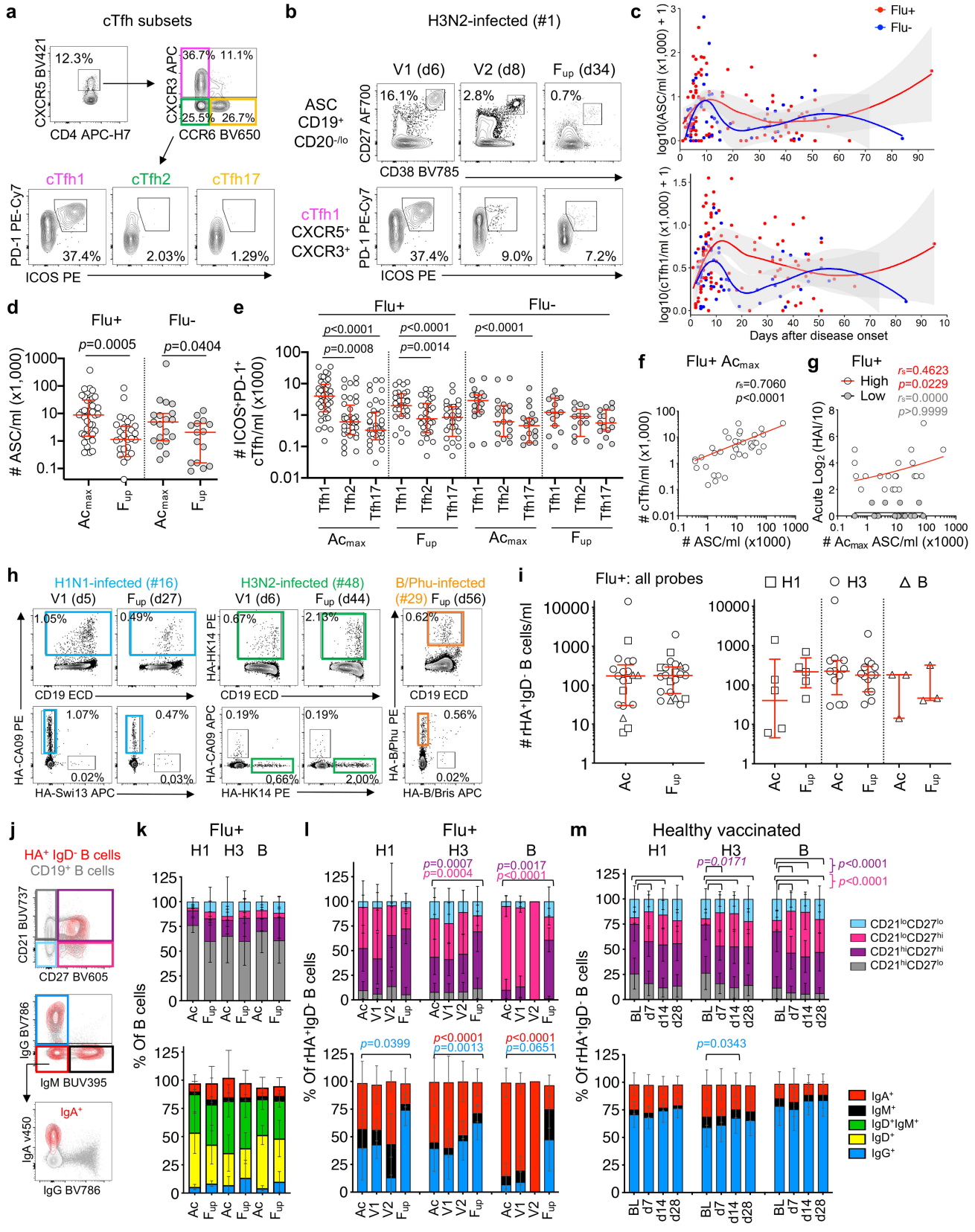

Figure 3 Nguyen *et al.*

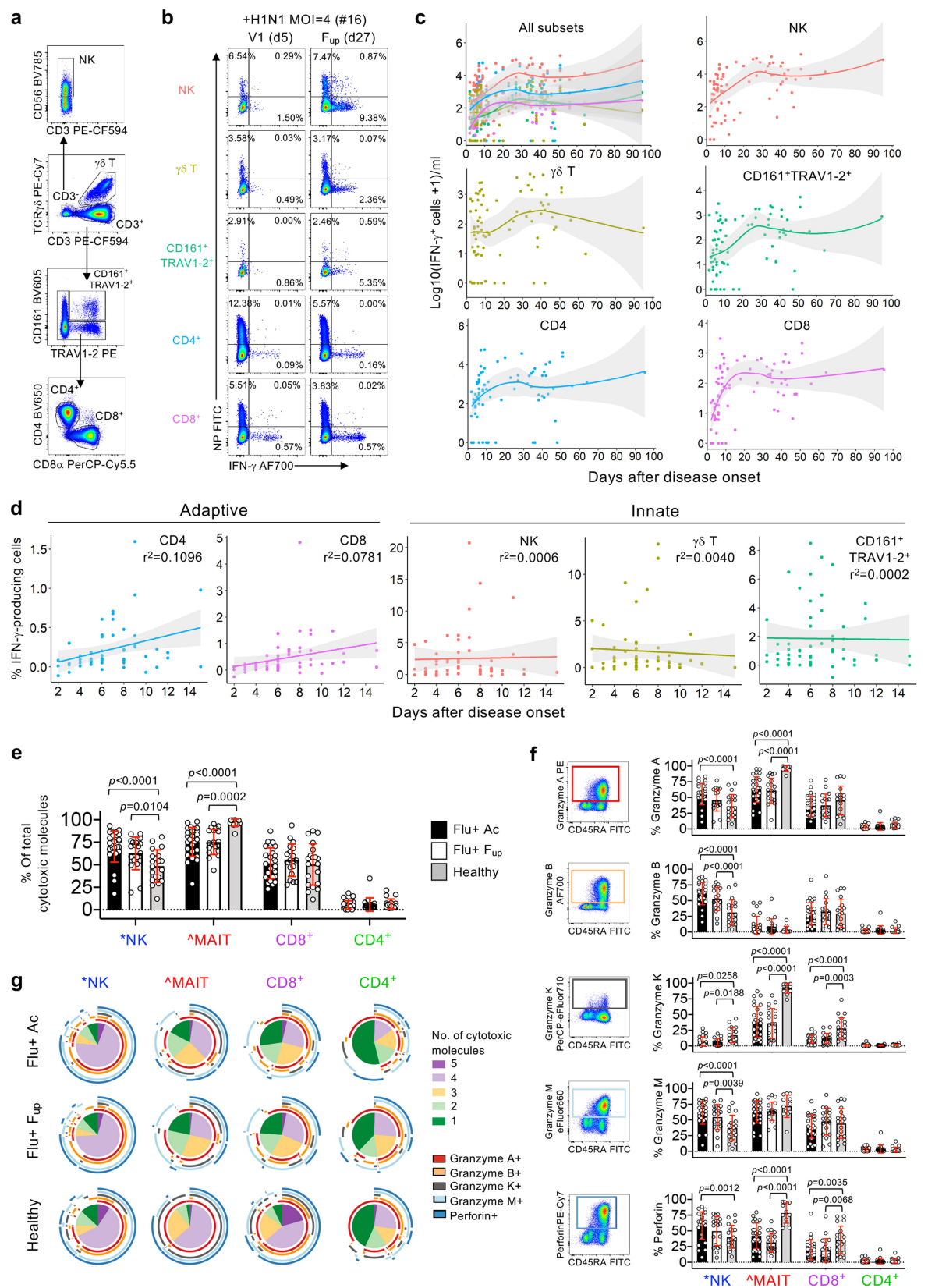

Figure 4 Nguyen *et al*.

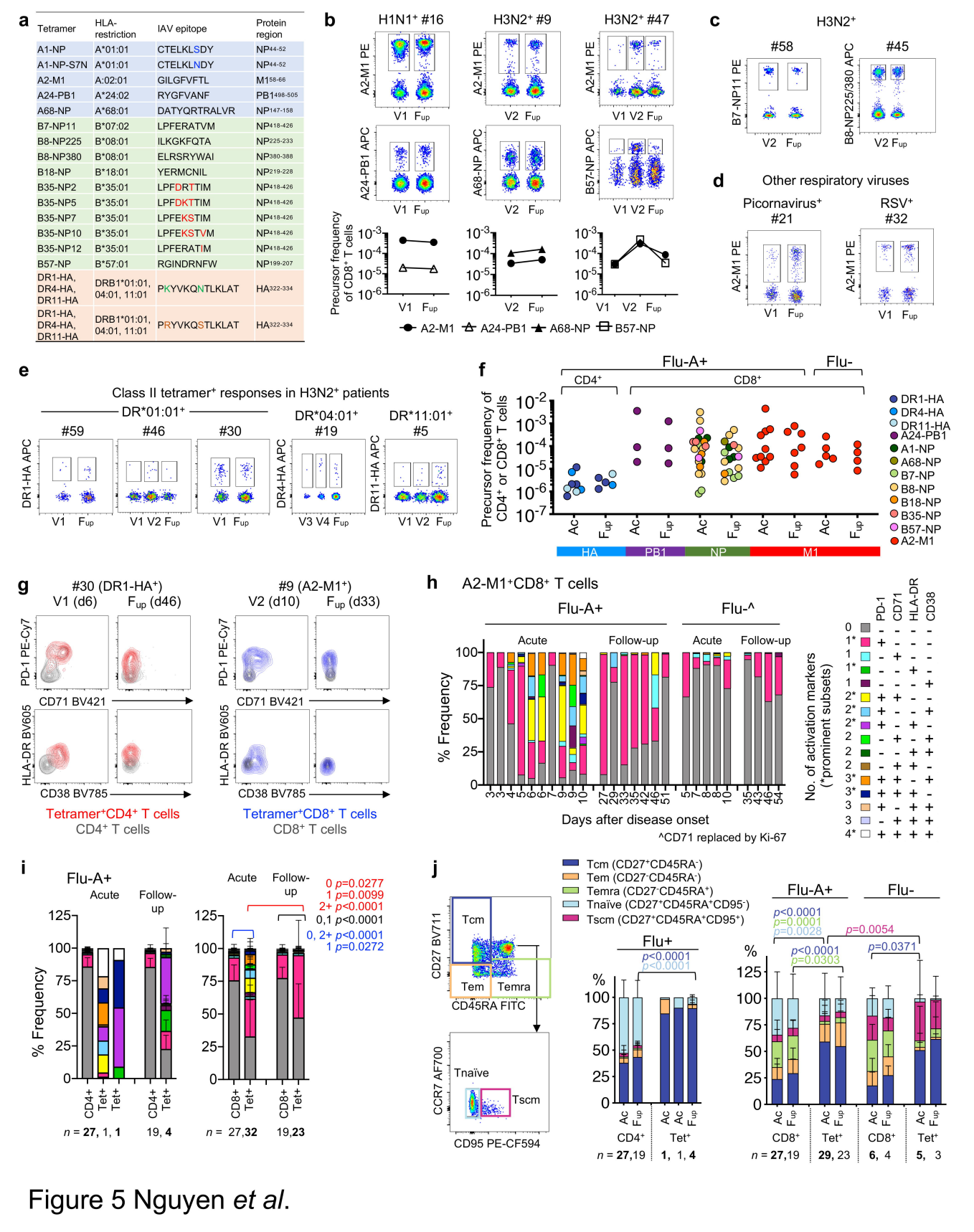

Figure 5 Nguyen *et al*.

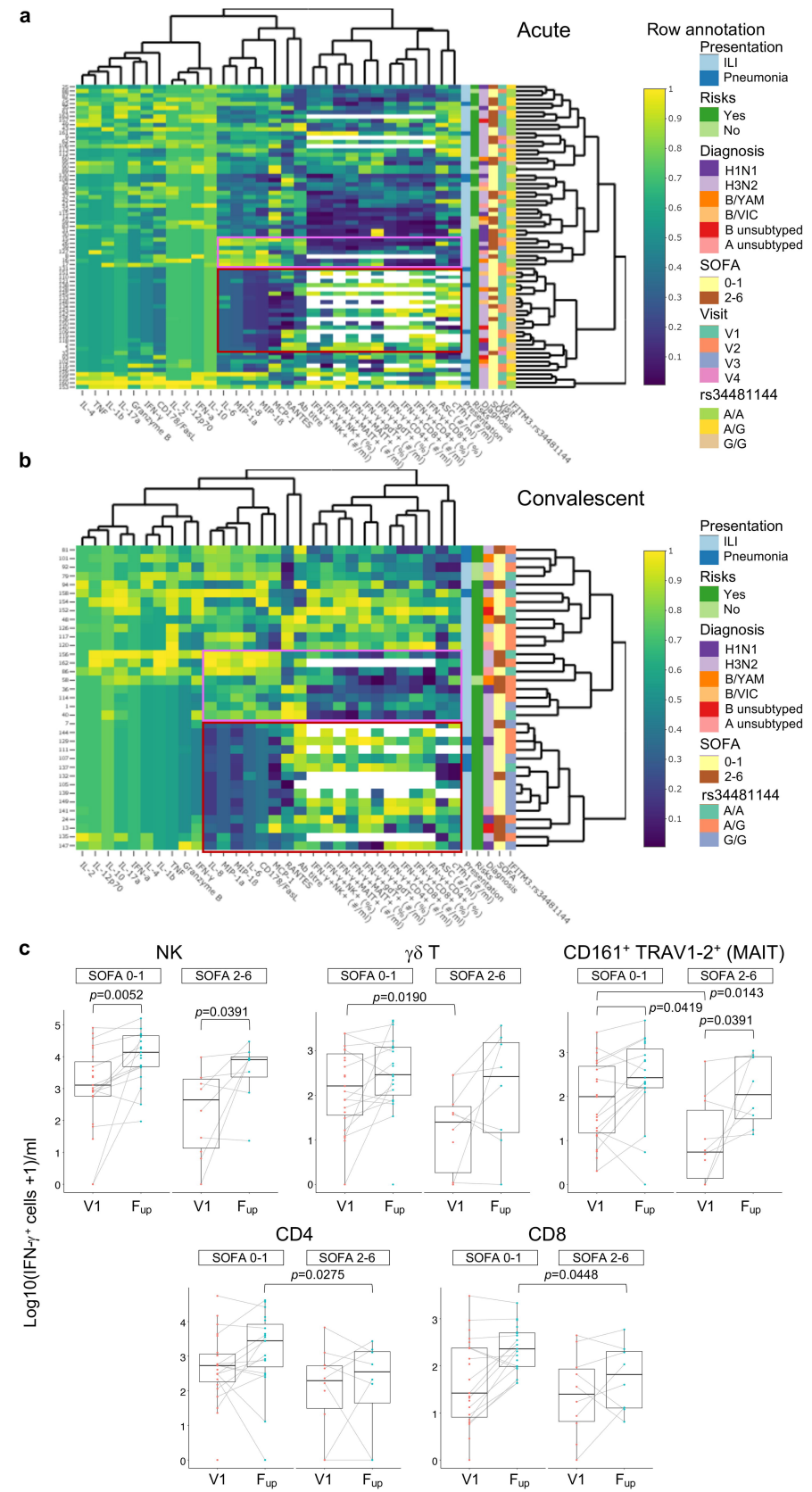

Figure 6 Nguyen *et al*.